Imaging of targets beneath foliage with SAR tomography

Matteo Nannini, Rolf Scheiber, Ralf Horn
German Aerospace Center (DLR), Microwaves and Radar Institute (HR), Oberpfaffenhofen, Germany.
e-mail: *matteo.nannini@dlr.de*

Abstract

SAR tomography (SARTom) is an imaging technique that allows multiple phase centre separation in the vertical (height) direction, leading to a 3-dimensional (3D) reconstruction of the imaged scene. It is usually performed after standard 2D SAR repeat-pass processing and operates on a stack of coregistered SAR images. Retrieval of volume structure information (e.g. for forest classification) and the solution of the layover problem are two of the most promising applications. In this paper the application of SARTom to image targets hidden beneath foliage is presented. This method is applied to L-band airborne data acquired during a tomographic campaign that took place in September 2006 on the test site of Dornstetten (Germany) involving the E-SAR system of the German Aerospace Center (DLR).

1 Introduction

SARTom makes it possible to obtain a complete 3D representation of the scene. In [1] the first demonstration of airborne SAR tomography was carried out and the main constraints in terms of resolution and ambiguity rejection have been analysed. When the focusing step is performed by means of the Fourier beamformer, realistic working conditions, like non-uniform track distribution, could heavily impact on the final results. That is why in the recent years modern beamforming techniques like Capon and MUSIC have been used allowing higher ambiguity rejection and the possibility to outperform the Fourier resolution [2, 3]. Despite these drawbacks, the advantage of the Fourier beamformer is that it maintains the signal phase (which is important for further polarimetric and interferometric evaluation) and it is used as a reference in order to plan the acquisition geometry. Through it the relation between the height resolution ρ and the tomographic aperture dimension L_{tomo} is:

$$\rho = \frac{\lambda\, r_0}{2\, L_{tomo}}, \tag{1}$$

where r_0 is the master slant range distance. In order to avoid ambiguities within a maximum volume height V, the averaged baseline d must undergo:

$$d \leq \frac{\lambda\, r_0}{2\, V}. \tag{2}$$

Now joining (1) and (2) the required number of tracks is $N = \frac{L_{tomo}}{d} + 1$. These relations were used in order to plan a tomographic campaign that took place in Dornstetten (Germany). Its goal was to analyse the potential of SARTom for extracting information concerning targets hidden beneath the foliage.

The objective of this paper is twofold: to present the first tomographic results concerning targets hidden beneath foliage and to perform a comparison between tomograms obtained in different polarization basis (lexicographic, Pauli) in order to analyse how polarimetry can enhance the target contribution in comparison to the canopy.

2 SARTom Processing

Standard 2D SAR processing is the first step for performing SARTom and it is carried out by means of the Extended Chirp Scaling algorithm [4]. Then, as shown in [5] a Height dependent Motion Compensation-Coregistration approach (HMCC) has to be performed in order to compensate for the SAR processing drawbacks related to a simple motion compensation-coregistration and to refer to nominal tracks. At this point beamforming techniques can be applied; we will refer to the Capon beamformer. The so-called steering vector $\boldsymbol{a}\,(h)$ is defined as:

$$\boldsymbol{a}\left(\hat{h}\right) = \exp\left(j\frac{4\,\pi}{\lambda}\boldsymbol{R}_{\hat{h}}\right) \tag{3}$$

with $\boldsymbol{R}_{\hat{h}} = \left[R_1(\hat{h}), \cdots, R_N(\hat{h})\right]$ representing the distances sensors-target for a height $\hat{h}$. After the sample complex covariance matrix computation:

$$\boldsymbol{R} = \frac{1}{N}\sum_{k=-N/2}^{N/2} \boldsymbol{s_t}(k)\; \boldsymbol{s_t}(k)^H, \tag{4}$$

the Capon beamformer can be applied:

$$\boldsymbol{C}(h) = \frac{1}{\boldsymbol{a}^H\,(h)\;\; \boldsymbol{R}^{-1}\; \boldsymbol{a}\,(h)}. \tag{5}$$

By scanning the image stack in the azimuth direction a 3D density reconstruction as a function of height and azimuth can be presented in a tomogram.
Selecting different polarization channels and basis, it is now possible to produce tomograms as a function of the polarization ([6, 3]). In this way the physical characteristics of the media with which the electromagnetic wave interacts can be understood.

3 The experiment

The data set has been acquired in September 2006 close to Dornstetten (Germany) in L-band.
Some targets of interest (vehicles, containers, corner reflectors) have been located inside and outside the forest in order to evaluate the impact of the canopy on the target response. The area where the experiment took place is relatively flat and half of the region is covered by non-homogeneous forest stands related to different species. The tree height is ranging between 10-30m.

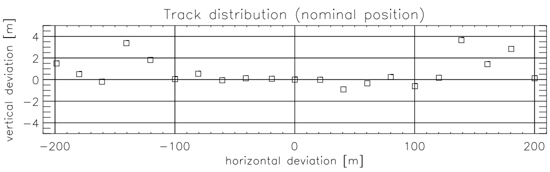

Figure 1: Dornstetten experiment: acquisition geometry.

The acquisition geometry is a regular horizontal grid of 21 tracks with an average baseline of 20m. As it is possible to observe from **Figure 1**, the actual acquisition geometry is very close to the planned one, with a maximum deviation of around 4m between nominal and real track. The choice of a large tomographic aperture results in an average tomographic resolution of 2m.

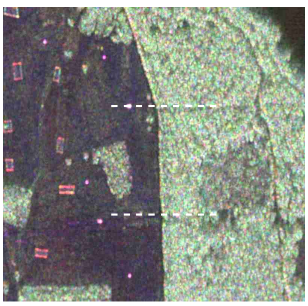

Figure 2: Full polarimetric SLC image (400m x 400m). Coding: RGB (HH, HV, VV). The two cuts along which the tomographic processing is carried out are depicted (dashed lines).

In **Figure 2** the relevant subset of the full polarimetric SLC image in the RGB coding (HH,HV,VV) is reported. The tomographic processing results presented next were carried out along the two cuts depicted in the azimuth direction.

4 Tomographic results

This section presents the tomographic SAR processing results. The first profile includes two trucks (recalling that one is outside the forest and the other is located inside it) and the second a container. In the next section tomograms obtained by means of the Capon beamformer will be presented in the HH polarization. Then, the impact of polarization will be examined by changing the polarization channel and the polarimetric basis. Results obtained by means of a coherent beamformer will also be presented.

4.1 HH polarization

Figure 3 represents the tomogram related to the trucks. It is possible to see that the two trucks are visible along the azimuth coordinate. The first spot represents the truck outside the forest and second the one inside it. The canopy over the second truck is also clearly visible.

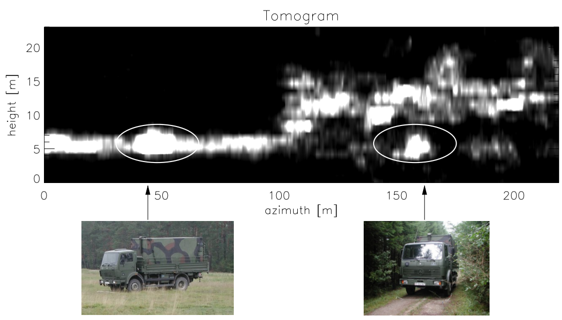

Figure 3: Tomogram in the HH polarization representing two trucks: one outside and the other inside the canopy.

It is worth noting that the truck inside the forest is not visible in the single SAR image but through the help of several acquisitions SARTom can detect it. A few observations concerning the tomogram itself can be made: the absence of the ground under the canopy is due to the fact that the ground-trunk double bounce reflection is missing because the truck has been placed on a small track inside the forest on which no trees were present. Without these reflections, the backscattered power related to a terrain contribution is much less than the one from the canopy or the hidden target.

In **Figure 4** the tomogram related to the container is reported. The container as well as the canopy is visible.

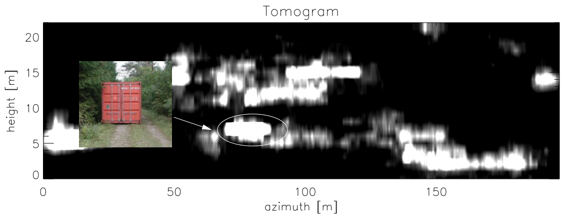

Figure 4: Tomogram in the HH polarization representing the container inside the forest.

The forest height corresponds to the actual one and also for this target the same consideration can be done for the absence of the ground component.

4.2 Polarimetric comparison

In this section the impact of polarization on SARTom will be analysed. Due to the heterogeneity of the scene and the presence of different kind of scattering mechanisms (natural, man-made scatterers), polarimetry is useful to extract the target contribution. First the tomographic results will be presented in the lexicographic basis.

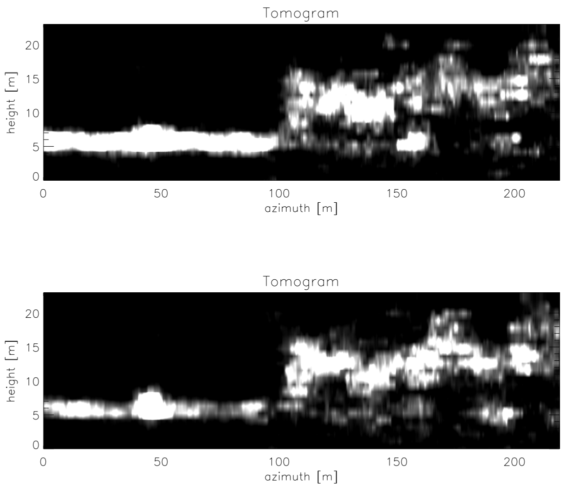

Figure 5: Tomogram of the profile related to the two trucks. (top) VV polarization (bottom) HV polarization.

Figure 5 represents the profile of the azimuth cut related to the trucks. Comparing **Figure 3** with **Figure 5(top)**, it is possible to observe that the HH and the VV polarization provide similar results. Examining now the cross-polarized channel (**Figure 5(bottom)**), one can observe that the target contribution disappeared, probably due to the higher sensitivity of the HV channel to volumetric structures, that does not allow to receive a backscattered signal from the target with significant power.
The same analysis can be carried out for the azimuth cut related to the container. In this case the backscattered signal related to the target in the cross-polarized channel is not negligible as for the previous case. In fact, the tomograms related to the three channels present no differences in a qualitative analysis; for this reason and because of the lack of space the related tomograms will not be reported.
Let us now consider the Pauli decomposition that allows a first direct interpretation of the scattering mechanisms. In order to generate tomograms in the Pauli basis, the SLC images related to different channels have been first combined and then the tomographic processing has been carried out. The well known form of the scattering vector related to this basis is (for the monostatic case)

$$\begin{aligned} \overrightarrow{k}_{3P} &= \left[S_{hh}+S_{vv}, S_{hh}-S_{vv}, 2\,S_{hv}\right]^T/\sqrt{2} \\ &= \left[P_1, P_2, P_3\right]^T, \end{aligned} \tag{6}$$

where S_{ij} corresponds to the SLC image in the ij polarization. The peculiarity of this basis is that the first element emphasizes the odd bounce contributions, while the second element the even ones. Concerning the third element it is, as for the lexicographic basis, related to volumetric contributions.
Considering the profile related to the trucks, the first and the second element of the Pauli basis are reported in **Figure 6**. It is possible to observe that for this target, the use of this basis allows to identify some features that are not represented in the lexicographic one. For the truck under foliage the P_1 response is stronger for the frontal part of the truck itself while, the P_2 component, has a stronger answer for the rear part of it. For the P_3 contribution refer to **Figure 5(bottom)**.

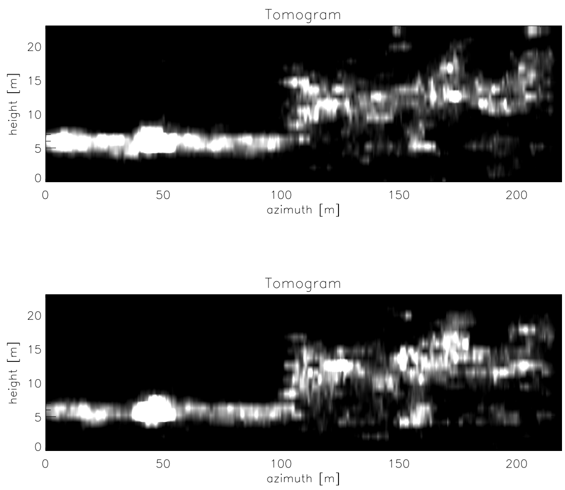

Figure 6: Tomogram of the profile related to the two trucks in the Pauli basis. (top) P_1 (bottom) P_2.

Concerning the container, also for the Pauli basis, the P_3 response is very similar to the P_1 and P_2 contributions (for this reason it will not be shown). It should be expected that the double bounce response related to this target (emphasized by the P_2 component) presents higher amplitude when compared to other scattering mechanisms.

4.3 Coherent Beamforming

In order to exploit completely the polarimetric information, the Capon beamformer cannot be used because the amplitude of its response is more an indication of the scatterer position rather than a measure of its backscattered power. For this reason, it is necessary to make use of a coherent beamformer [7], that despite its reduced resolution and ambiguities rejection characteristics allows to combine directly the tomograms and refer them to their total power. For the coherent beamformer, the tomograms can be presented in an RGB coded image that will allow to identify the main scattering mechanisms.

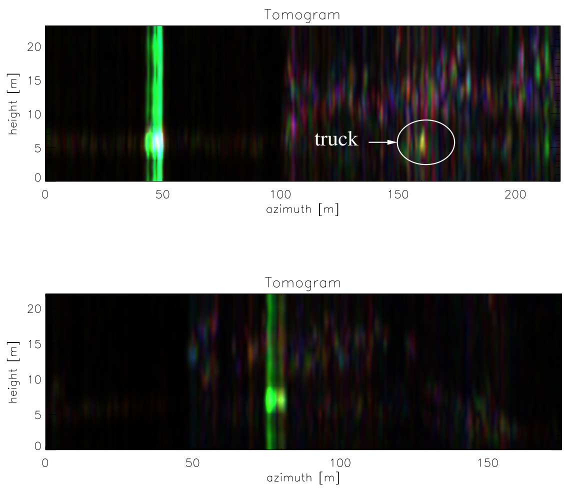

Figure 7: Full polarization tomograms in the Pauli basis by means of the coherent beamformer with a Hamming apodization. Coding: RGB (P_1, P_2, P_3). (top) Trucks (bottom) container.

The Pauli tomograms related to the two scenarios (trucks, container) are reported in **Figure 7**. Observing **Figure 7(top)** it is possible to note that the double bounce contribution is the main one concerning the target outside the forest. For the hidden truck, the power of the P_3 component is much less than the one related to the other two components (the truck corresponds to the yellow spot). If now the polarimetric tomogram related to the container is examined (**Figure 7(bottom)**), it is possible to observe that, as expected, the P_2 contribution related to double bounce reflections is the one with higher power when compared with the other two. It has to be commented that the reduced azimuth dimension of the targets, when compared to the tomograms obtained by means of the Capon beamformer, depends on the fact that for the coherent beamformer there is no need to compute the sample covariance matrix. Therefore the typical spreading effect of the Capon beamformer is not present. The image saturation depends on the strong backscattered power of the main target present in the scene.

5 Conclusion and future work

In this paper first experimental results concerning 3D imaging of targets beneath foliage have been presented. A stable response of the tomographic technique makes it possible to represent both the target and the canopy with height information comparable to the ground truth measured at the test site.
The use of the coherent beamformer allows, especially for the case of the container, to exploit completely the polarimetric information and associate a signature to the target that can be exploited in order to detect it. Anyhow, concerning the trucks, due to the reduced cross-polarization power also the Capon beamformer allows the identification of the target beneath foliage.

6 Acknowledgements

The authors would like to thank eOsphere Limited and the Electro-Magnetic Remote Sensing Defence Technology Centre for their support of this work as well as the E-SAR team of DLR for their efforts in conducting the campaign.

References

[1] A. Reigber and A. Moreira, *First Demonstration of Airborne SAR Tomography using Multibaseline L-Band Data*, IEEE Trans. on Geosc. and Remote Sensing Vol. 38, no.5, pp.2142-2152, 2000.

[2] F. Lombardini and A. Reigber, *Adaptative spectral estimation for multibaseline SAR Tomography with airborne L-band data*, in Proc. IGARSS, Toulouse, France, 2003.

[3] S. Guillaso and A. Reigber, *Scatterer Characterisation Using Polarimetric SAR Tomography*, in Proc. IGARSS, Seoul, Korea, 2005.

[4] A. Moreira et al., *Extended Chirp Scaling Algorithm for Air- and Spaceborne SAR Data Processing in Stripmap and ScanSAR Imaging Modes*, IEEE Trans. on Geosc. and Remote Sensing Vol. 34, no.5, pp.1123 - 1136, 1996.

[5] M. Nannini and R. Scheiber, *Height Dependent Motion Compensation and Coregistration for Airborne SAR Tomography*, in Proc. IGARSS, Barcelona, Spain, 2007.

[6] A. Reigber, *Airborne Polarimetric SAR Tomography*, PhD thesis, University of Stuttgart, Germany, 2001.

[7] M. Nannini and R. Scheiber, *A Time Domain Beamforming Algorithm for SAR Tomography*, in Proc. EUSAR 2006, Dresden, Germany, 2006.